Journal of Marine Research, 63, 563–577, 2005

Dynamics of a CO_2-seawater interface in the deep ocean

by Joakim Hove[1] and Peter M. Haugan[2]

ABSTRACT

A trough filled with liquid CO_2 located at 3940 m depth has been used as a model system for CO_2 deposition on the seafloor. To study the intrinsic properties of the interface between CO_2 and seawater a wave maker was used to excite regular plane waves. The frequency ($\lesssim$2.5 rad/s) and wavelength (20 cm–40 cm) of the waves have been measured, and compare reasonably well with the dispersion relation for deep fluid gravity waves. The shear stability of the interface was investigated by setting the water above the CO_2 in motion with a thruster. For shear velocities exceeding $v_c \simeq$ 17.6 cm/s the interface became unstable, with breaking waves and CO_2 droplets torn from the wave crests. For the sheared system we find that the energy spectrum of the interface variations has a peak for wavelength $\simeq$0.8 cm, meaning that energy absorption is greatest for this wavelength. For the most unstable wavelength of the Kelvin-Helmholtz instability to match this wavelength, an effective interfacial tension of the hydrate covered interface of $\gamma \simeq 0.075$ N/m must be assumed.

1. Introduction

It is widely accepted that enhanced CO_2 emission to the atmosphere affects the climate, and during the last twenty years many different means of stabilizing the CO_2 level have been investigated. Storage in the oceans has been considered, since this is the largest potential sink for anthropogenic CO_2 (Marchetti, 1977).

Options which have been investigated for CO_2 storage in the oceans include sinking lumps of hydrate (Lee *et al.,* 2003), various approaches based on gravitational currents from heavy CO_2 enriched water (Haugan and Drange, 1992) and droplet plumes (Alendal and Drange, 2001). On the Norwegian continental shelf, the oil company Statoil has injected gaseous CO_2 into geological structures since 1995 (Baklid *et al.,* 1996).

Due to the higher compressibility, liquid CO_2 is more dense than seawater for depths exceeding ~3000 m, and recently investigations of the feasibility of storing CO_2 in pools on the seafloor have begun (Brewer *et al.,* 1999). This paper reports about the latest investigation of this kind, with the main emphasis on the properties of the interface between CO_2 and seawater.

From an application point of view the key question is: "How stable is the CO_2 pool?" In

1. Bergen Center for Computational Science, University of Bergen, Allégaten 55, N-5007 Bergen, Norway. ***email: hove@ift.uib.no***

2. Geophysical Institute, University of Bergen, Allégaten 70, N-5007 Bergen, Norway. ***email: haugan@gfi.uib.no***

order to begin to address this question, there is a need to describe and understand several aspects of the interface dynamics. Due to molecular diffusion, the seawater immediately above the interface will be enriched by CO_2, and this seawater will be dispersed by turbulence and ocean currents.

Ocean currents will induce waves in the interface. When the ocean currents are sufficiently strong we expect that the interface will become unstable with turbulent mixing. Whether this takes place at typical current speeds is an important question because mixing processes like this are generally orders of magnitude more efficient when there is turbulence (Kantha and Clayson, 2000). The experiment has been designed to simulate different ocean current regimes and their effect on the interface; simulations of abyssal CO_2 pools show that the interfacial properties are important for the outflux (Haugan and Alendal, 2005). Although the question of outflux of CO_2 from the pool is ultimately the most important question, the current experiment has not been designed to assess this in a quantitative fashion.

Brine pools, which are topographic depressions containing high-salinity water, are an interesting natural analogue. Studies indicate that for these systems the stratification is sufficiently strong to inhibit turbulent mixing, and consequently the salt in the pools is *not* dispersed out in the remaining seawater (Cappelen *et al.,* 1998; Anschutz *et al.,* 1999).

In the relevant (p, T) regime there will be a thin layer of hydrate (Sloan, 1998) on the interface between CO_2 and seawater. The physics and chemistry of this layer is a topic of intense research both experimentally and theoretically (Mori, 1998). The behavior of the hydrate layer is important, both for the hydrodynamic properties of the interface and for the transport of CO_2 across the interface. Apart from the value of the interfacial tension γ, which is affected by the hydrate layer, we will only discuss it qualitatively. For moderate shear stress, the hydrate will serve as a low permeability membrane and also dampen waves. When the wave-induced interfacial stress exceeds a certain limit, the membrane will be destroyed. This will probably lead to enhanced transport of CO_2 into seawater, both because the low permeability membrane is perforated and because the interfacial waves will be even more turbulent when the dampening hydrate layer is shredded.

In this paper we analyze results from an experiment performed in the Pacific off San Francisco, in October 2003, with the research vessel R/V *Western Flyer* and the ROV *Tiburon* of the Monterey Bay Aquarium Research Institute (MBARI). A trough was lowered to the seafloor and filled with liquid CO_2. The properties of the interface were studied by exciting surface waves with a wave maker and a thruster. The experiments have been interpreted in terms of two-liquid theory (Drazin and Reid, 1981; Chandrasekhar, 1961).

The rest of the paper is organized as follows: In Section 2 we briefly describe the experimental procedure, in Section 3 we summarize the measurements and describe the methodologies used to extract quantitative results. In Section 4 we discuss the results along with the relevant theory. Finally there is a brief conclusion in Section 5.

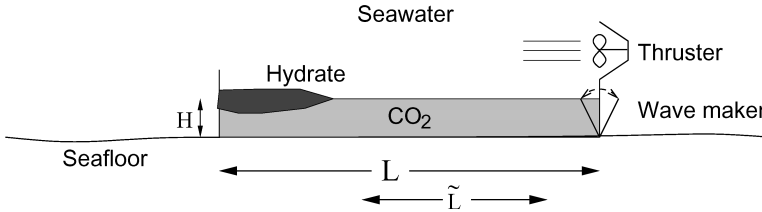

Figure 1. The trough with the thruster and the wave maker; only one was used at a time. The lump of solid hydrate located downstream was created incidentally but actually served as a very convenient *wave absorber.* The length $\tilde{L} \approx L/2$ corresponds to the part of the trough where the waves can propagate freely, without influence from either the hydrate or the wave maker.

2. Experiment

Due to the extreme depth the experiment was very complex to perform, requiring ingenious planning and engineering skills from the staff at MBARI and the ROV pilots. A detailed account of the experiment can be found in the companion paper (Brewer *et al.,* 2005). For the current paper, the experiment can be quite briefly summarized as follows: (1) a trough was lowered to the seafloor at 3940 m depth; (2) the trough was filled with about 661 of liquid CO_2; (3) waves were excited on the interface with a wave maker and a thruster and (4) measurements of the system were made. The experimental setup is shown schematically in Figure 1.

The measurements mainly come from video recordings of the interface. In addition, Conductivity Temperature Depth (CTD) measurements were continuously collected, a movable pH probe was used to do spatially-resolved pH measurements, and a special closed cell was used to study the dynamics of the H_2CO_3 dissociation process (Brewer *et al.,* 2005).

3. Results

The waves excited by the wave maker and the thruster were very different and will consequently be analyzed separately, starting with the results from the wave maker experiment.

a. Wave maker results

The wave maker is controlled by an applied voltage, V. This leads to oscillations with a temporal frequency $\omega(V)$ and propagating waves with wavelength $\lambda(V)$. For each applied voltage V, the wavelength has been measured from the images (see Fig. 2 for a representative example). Experiments were performed for $V = 1000, 1250, 2500, 3500, 5000$; for $V = 1000$ and 1250 the waves were not clear enough to measure ω and λ reliably.

The frequency ω was determined by considering the time series of the height $z(t)$ of the interface at a fixed point. Assuming that the plane wave description is correct we have

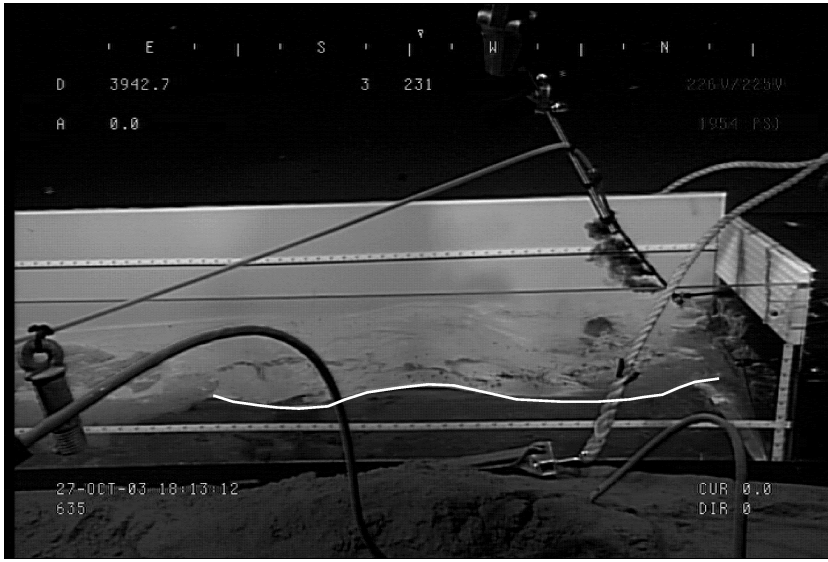

Figure 2. Figure showing regular plane waves on the CO_2-seawater interface, the white line is added to visualize the interface.

$$z(t) \sim A \cos(\omega t + \phi), \tag{1}$$

and ω was determined by a least squares fit to Eq. 1. The measured values of ω and λ are given in Table 1.

b. Thruster results

From the thruster experiment the main goal was to determine whether there was a lower critical shear velocity, v_c, such that the interface was turbulent for velocities exceeding this velocity. The video footage clearly confirmed this; at thruster setting 250 RPM the

Table 1. Numerical values for ω and λ. The error bars are estimated by repeating the measurement procedure on different time series. The measurements for $V \geq 2500$ are quite well described by the relations $\lambda(V) \sim \lambda_0 - \alpha \cdot V^2$ and $\omega(V) = \omega_0 + \beta \cdot V$, and the values given for $V = 1250$ and $V = 1000$ are inferred by extrapolating the results for $V \geq 2500$.

Voltage [arb. units]	ω [rad/s]	λ [cm]
5000	2.52 ± 0.10	19.6 ± 1.2
3500	1.88 ± 0.05	34.4 ± 3.4
2500	1.49 ± 0.04	40.3 ± 4.0
1250	0.98	45
1000	0.88	46

interface only contained moderate perturbations, whereas for 260 RPM it was highly turbulent. From this we inferred a critical value of 255 RPM, corresponding to $v_c = 17.6$ cm/s $\pm$ 1.1 cm/s. The major source of uncertainty in the final estimate comes from the RPM/velocity calibration. The supercritical interface resembled images of boiling lava, with breaking waves and CO_2 droplets torn off from the wave crests. For velocities exceeding v_c the interface was also surprisingly *isotropic.*

Turbulence is characterized by power law spectra (Kantha and Clayson, 2000), in particular this means that there is energy localized at short length and time scales. We have not been able to measure interfacial height directly, but the anisotropic lighting has given quite good visual contrast between peaks and valleys, and we have used *intensity variations* in the images as an indirect probe for energy. The spectrum $E(k)$ has been determined by wavelet analysis of the images.

Wavelet analysis (Addison, 2002) is a method which has been used with great success to do *spatially resolved* frequency analysis; i.e., a signal can be transformed to a representation with partial localization in both direct and reciprocal space. Consider a one-dimensional signal $\Omega(x)$ of dimensional length L and $N = 2^n$ measurements. Using the discrete Fast Wavelet Transform (FWT) this can be written as a mean and details at various length scales

$$[\Omega_1, \Omega_2, \Omega_3, \Omega_4, \Omega_5, \Omega_6, \Omega_7, \Omega_8] \xrightarrow{FWT} [\underbrace{S_3, T_{3,1}}_{\lambda=L}, \underbrace{T_{2,1}, T_{2,2}}_{\lambda=L/2}, \underbrace{T_{1,1}, T_{1,2}, T_{1,3}, T_{1,4}}_{\lambda=L/4}]. \quad (2)$$

In Eq. 2 S_3 is the mean of the signal, and the coefficients, $T_{k,l}$, denote the details at length scale $\lambda_k = L2^{k-n}$ and location $l\lambda_k$. The sum

$$E(\lambda_k) = \sum_{l=1}^{2^{n-k}} T_{k,l}^2 \quad (3)$$

is then an indicator of the total energy at length scale λ_k. With increasing shear we expect that the interface will contain more energy, in particular at the short length scales.

To analyze the energy content of the interface we have cropped the images to 128 $\times$ 128 pixel grayscale images without visible experimental apparatus (see Fig. 3 for an example of the rawdata used for the quantitative image analysis). The FWT was then applied to the images, and we calculated the spectrum according to Eq. 3. The images were sampled with a frequency of 2 Hz and the results from a total of 20–40 consecutive images were combined to form mean and standard error.

Figure 4 shows the average energy according to Eq. 3 for different length scales and shear velocities. Figure 5 shows the same data, plotted as a function of shear velocity. This figure indicates a transition at $v_c \approx 17.6$ cm/s, consistent with the video footage.

Figure 3 shows typical black and white images of the interface. As we can see, there is a distinct anisotropy in the images with more variations in the cross trough

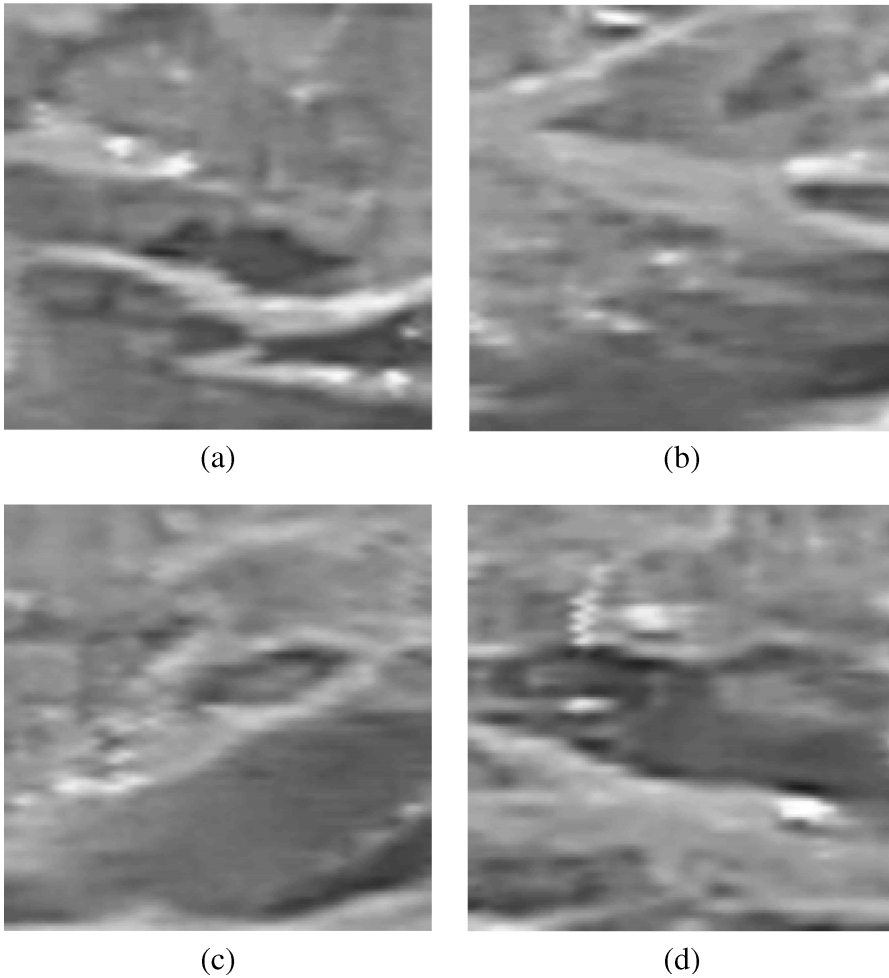

Figure 3. Black and white images of the interface for the four thruster settings (a) 200, (b) 250, (c) 260 and (d) 275. RPM, corresponding to shear velocities of about 13.0 cm/s, 17.1 cm/s, 18.0 cm/s and 19.2 cm/s. The critical value was ≈255 RPM, i.e. 17.6 cm/s. These images are examples of the "rawdata" used in the Wavelet analysis to obtain the spectrum $E(\lambda_k)$ according to Eq. 3.

direction. The origin of this anisotropy is most likely the relative orientation of the illumination and the camera and *not* due to a real physical anisotropy. In fact the interface itself was surprisingly *isotropic,* particularly above the critical velocity. Figures 6 and 7 show spectra analogous to those in Figures 4 and 5, but only vertical (cross trough) lines have been analyzed in a 1-d approach. Figures 6 and 7 show roughly the same results as those in Figures 4 and 5 but the threshold behavior is slightly more prominent.

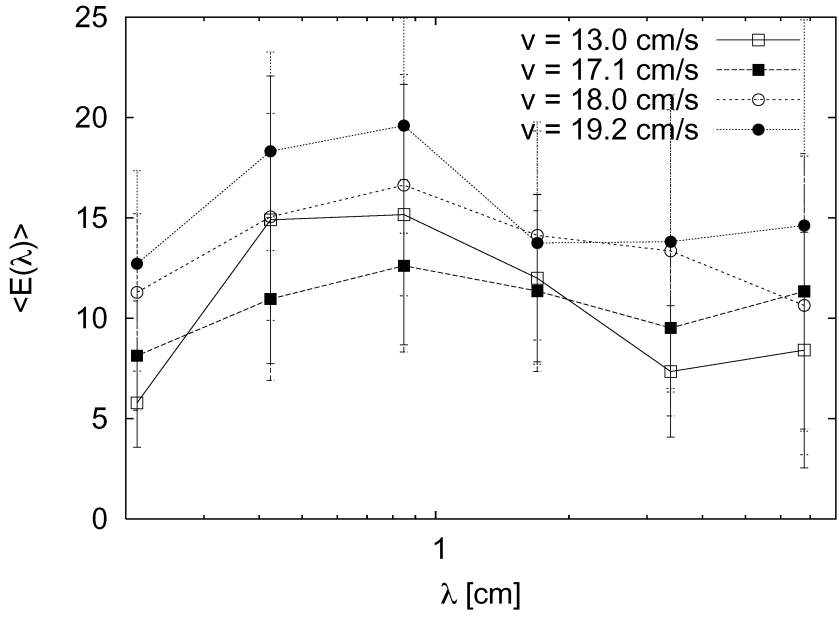

Figure 4. The average "energy" at different length scales, λ, for thruster experiment with different values of the shear. Each datapoint is the average of the results from 20–40 images, and the error bars are the *standard error.*

4. Discussion

a. Wave maker experiment

There will be a thin, $t \sim 10^{-6}$ m–10^{-5} m layer of hydrate (Mori, 1998) on the interface between the CO_2 and seawater. Since we will be considering waves with amplitude $A \gg t$ it is justified to ignore the finite thickness of the hydrate layer, and consider CO_2 and seawater as a *two-layer* system. The hydrate film is in a dynamic equilibrium, continuously formed and dissolved on a time scale which is instantaneous compared to the frequency of the wavemaker (Mori, 1998). Due to the dynamic nature of the hydrate, it will present a much smaller stretch resistance than an inert membrane covering the interface.

Waves with amplitude $A \ll h$ where h is the depth, can be described by linear theory (Kantha and Clayson, 2000). For the current experiment we have $A \lesssim 3$ cm and $h = 11$ cm and we have exclusively used the theory for linear wave propagation. Since we are considering a two-layer problem where $\rho_1 \approx \rho_2$ the dispersion relation must take the perturbations of both layers into account, giving the *two-layer* dispersion relation (Baines, 1995),

$$\omega = \sqrt{\left(\frac{kg\Delta\rho}{\rho} + \frac{k^3\gamma}{\rho}\right)\left(\frac{\tanh kh}{1 + \frac{\rho_2}{\rho_1}\tanh kh}\right)} \simeq \sqrt{\frac{g\Delta\rho k}{2\rho}} = \sqrt{\frac{g'k}{2}}. \qquad (4)$$

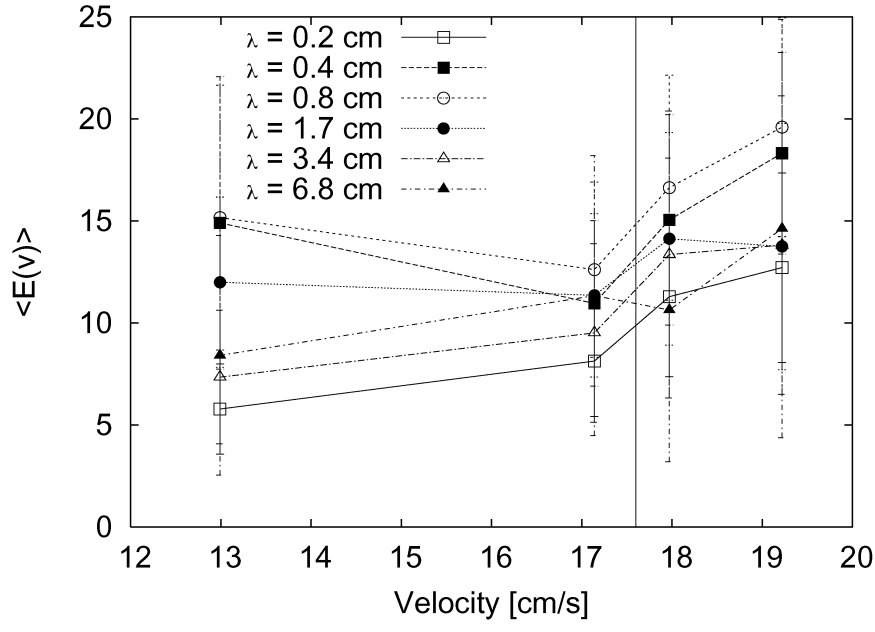

Figure 5. Similar to Figure 4 but plotted as a function of shear velocity, at fixed length scale.

In Eq. 4 we have assumed that with total depth, $d \approx 4000$ m, we can safely set $\tanh kd = 1$. The approximation on the right-hand side of Eq. 4 applies in the regime

$$2\pi\sqrt{\gamma/g\Delta\rho} \ll \lambda \ll 2\pi h.$$

The waves excited by the wave maker were in the range $20\text{ cm} \lesssim \lambda \lesssim 40\text{ cm}$. Eq. 4 involves *two* approximations; ignoring the surface tension amounts to describing the waves as gravity waves, this is the long wavelength approximation. Replacing $\tanh kh$ with unity is the *deep water approximation,* which is valid for short wavelengths. In the worst case these approximations lead to an error in ω of about $\pm 5\%$. Figure 8 shows the measured points of the dispersion relation (numerical values in Table 1), along with the curve corresponding to Eq. 4.

If we assume that the dispersion relation Eq. 4 *should* apply in the large k limit, Figure 8 still shows that there are seemingly significant quantitative deviations. In Eq. 4 the CO_2 density is the dominating uncertainty. We have used the values $\rho_{CO_2} = 1077\text{ kg/m}^3$ from Span and Wagner (1996); for ρ_{SW} we have used $\rho_{SW} = 1047\text{ kg/m}^3$. Observe that since

$$\Delta\rho = \rho_{CO_2} - \rho_{SW} \ll \rho_{CO_2},$$

the *relative* uncertainty in the determination of g' is quite large. An experimental uncertainty of $\pm 2\%$ in the determination of ρ_{CO_2} is sufficient to explain the deviations in

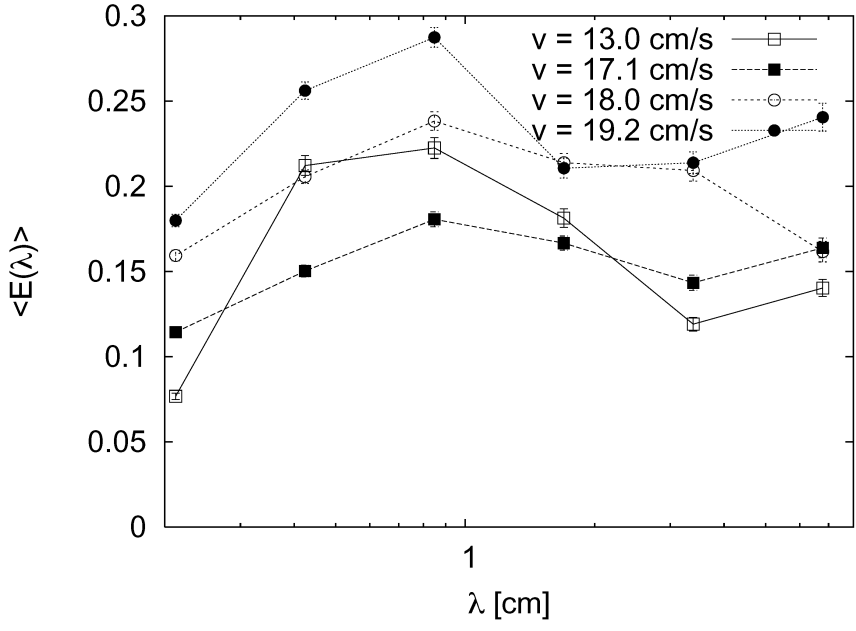

Figure 6. Similar to Figure 4 but only for one-dimensional lines across the trough.

the large k region of Figure 8; however, the value from Span and Wagner (1996) is quoted with an uncertainty of $\approx \pm 0.5\%$, so this is not sufficient to explain the disagreement.

In Eq. 4 the effect of the hydrate layer is to change the value of the surface tension γ; however, the hydrate layer is a *material phase* with its own dynamics. In particular wave motion leads to continuous breaking and regrowing of the hydrate layer. This process, which takes place in a thin layer immediately beneath the surface, leads to dissipation (Lucassen-Reynders and Lucassen, 1970). Unfortunately the trough was too short to reliably measure the decay rate of the waves, but a *very similar* experiment performed with grease ice gave a decay rate proportional to k^2 (Martin and Kauffman, 1981).

b. Thruster experiment

The motivation of the thruster experiment was to simulate the effect of ocean currents on the CO_2 surface. Generally the stability of a stratified interface increases with the density difference across the interface and the width of the transition layer. Linear stability analysis predicts stable flow when the Richardson number, R_i, satisfies (Kantha and Clayson, 2000)

$$R_i = \sqrt{-\frac{g}{\rho_{CO_2}}\frac{\partial \rho}{\partial z}}\left(\frac{\partial v}{\partial z}\right)^{-2} \simeq \sqrt{\frac{g\Delta\rho}{\rho_{CO_2}\Delta z_\rho}}\left(\frac{\Delta z_v}{\Delta v}\right)^2 \gtrsim 0.25. \quad (5)$$

The length scale for density variations, Δz_ρ, is very short and for the following discussion we will use $\Delta z_\rho = 0.1$ cm. We have not measured the velocity profile above the interface,

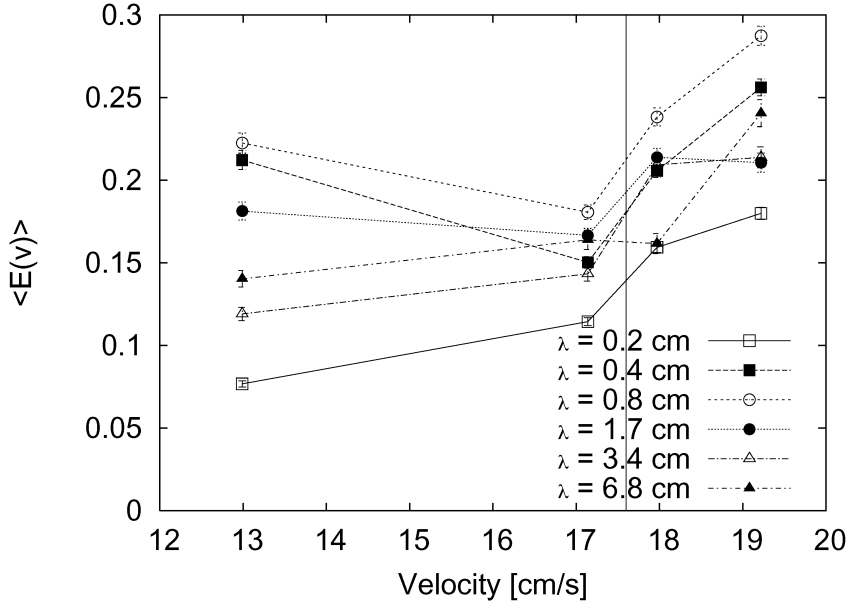

Figure 7. Similar to Figure 5 but only for one-dimensional lines across the trough.

but a rough estimate from studying the images indicates that the width of the transition layer is © (1 cm). Using the critical velocity $v_c = 17.6$ cm/s and solving Eq. 5 for the length scale of velocity variations, Δz_v, gives $\Delta z_v \approx 2$ cm.

Figures 5 and 7 confirm the idea of a critical velocity v_c; however, the anticipated spectrum changes do not really bear through. Instead of marked increase in the density of high frequency modes, Figures 4 and 6 show that $E(\lambda)$ increases quite uniformly when the shear velocity increases, except maybe for the longest wavelength $\lambda \approx 6.8$ cm whereas Figures 5 and 7 actually show a small *decrease* in $E(\lambda)$ when the critical velocity is exceeded.

When sheared, some of the interfacial modes might become unstable. Assuming that the rate of growth/decay is small, we can use *linear* stability analysis around the stable situation. This gives the following (Drazin and Reid, 1981) *growth rate* as a function of wavenumber k

$$S_r(k) = \frac{k}{\rho_1 + \rho_2} \sqrt{\rho_1\rho_2\Delta U - (\rho_1 + \rho_2)\left(\frac{g(\rho_1 - \rho_2) + k^2\gamma}{k}\right)}, \quad \Delta U = U_2 - U_1 \quad (6)$$

where index 1 indicates CO_2 properties and index 2 indicate seawater properties. If we differentiate this with respect to k, we find that the *maximal* growth rate is for wavelength

$$\lambda^* = \frac{2\pi(\rho_1\rho_2\Delta U - \sqrt{\rho_1^2\rho_2^2\Delta U^2 - 3g\rho_1^2\rho_2\gamma - 3g\rho_1^3\gamma + 3g\rho_2^3\gamma + 3g\rho_2^2\rho_1\gamma)}}{g\rho_1^2 - g\rho_2^2}. \quad (7)$$

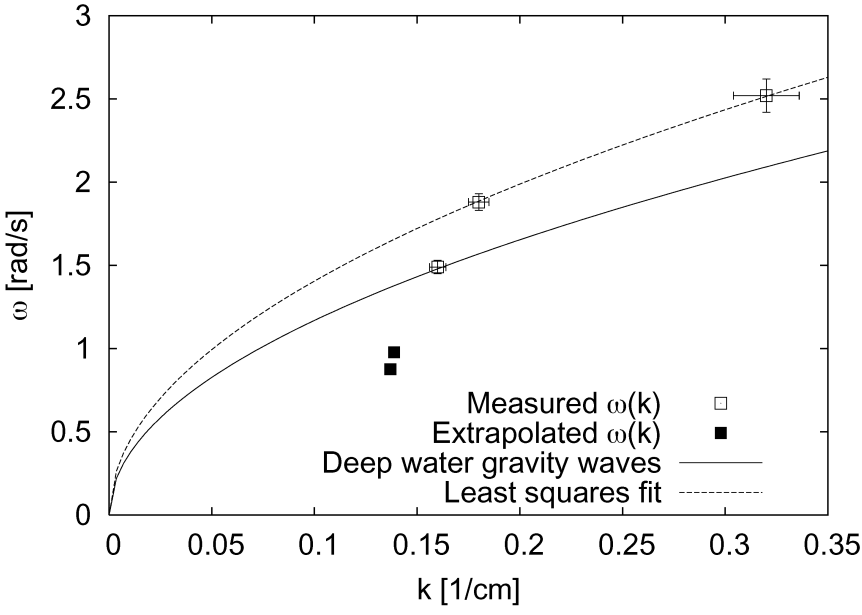

Figure 8. Measurements of k and ω, along with the theoretical curve Eq. 4 (dashed line), and a least-squares fit of the model, $\omega = \sqrt{g'k}$, for the two largest k values (see also Table 1).

If we assume that the peak in the spectrum, $E(\lambda)$, is located at λ^*, we can estimate λ^* from Figures 4 and 6.

Figures 9 and 10 show the growth rate (Eq. 6) and λ^* (Eq. 7), respectively. If we assume that λ^* corresponds to the location of the peaks in Figures 4 and 6, we can use Figures 9 and 10 to infer a γ value of $\gamma \simeq 0.075$ N/m. For this value of γ, the growth rate has quite a broad peak for $0.6\,\text{cm} \lesssim \lambda \lesssim 1.1\,\text{cm}$. The spectrum shown in Figures 4 and 6 are necessarily *broadened* by nonlinear interactions; however, we do not believe they are *shifted.* Yamane *et al.* (2000) measured the strength of the hydrate membrane to be about 0.10 N/m in temperature and pressure conditions similar to those of the experiment. The membrane strength is different from, but related to, the interfacial tension involved in Kelvin-Helmholtz instability. The value we suggest, 0.075 N/m, is smaller than, but quite similar to the one reported by Yamane. It is also similar to, but larger than, measured values of 0.02–0.03 N/m of interfacial tension between liquid CO_2 and seawater measured at similar depths (Uchida *et al.,* 2003).

As already mentioned, the experiment has not been designed to measure the loss rate from the pool. However, one qualitative observations in this regard is the following: using a movable pH probe we found background values with the pH probe located approximately 0.2 cm above the interface. This indicates that the diffusive flux under calm conditions is very low and that turbulent events are important for the total flux. During our experiment we measured background current speed of the order $\lesssim$10 cm/s; i.e., significantly below the

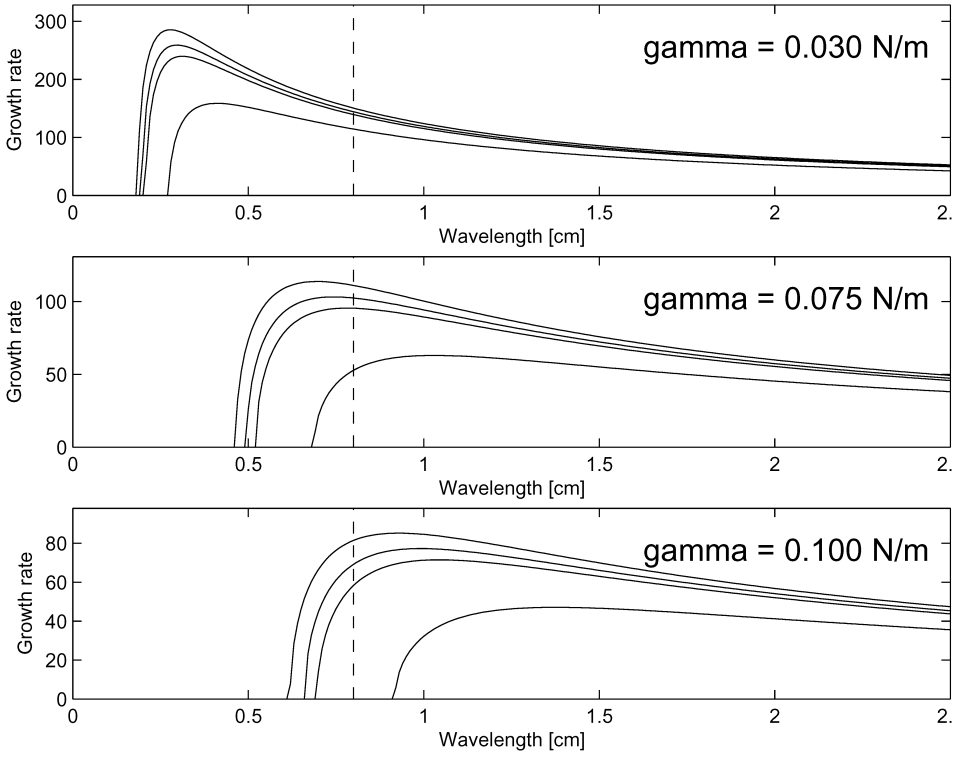

Figure 9. The growth rate as a function of wavelength. The different curves in each plot correspond to the shears: $U_2 - U_1 = [13.0$ cm/s, 17.1 cm/s, 18.0 cm/s and 19.2 cm/s]. The dashed vertical line corresponds to the wavelength, $\lambda = 0.8$ cm, inferred from Figures 4 and 6.

critical value for the onset of turbulence. The experiment was part of an ongoing project and hopefully future experiments will be able to assess the outflux more quantitatively. We note that experimental results are available in the literature for dissolution rate of hydrate-covered droplets and CO_2 hydrate (Brewer *et al.,* 2002; Rehder *et al.,* 2004) at 1000 m depth or less. For a liquid-CO_2 lake at the deep seafloor, only model estimates are available (Haugan and Alendal, 2005; Fer and Haugan, 2003). The model estimates of change in CO_2 level range from less than 10 cm per year at low flow speeds to several meters per year with currents of about 20 cm/s or more. These models seem able to capture the transition between laminar and turbulent conditions in the boundary layer when the current speed increases. However, they do not simulate the violent break-up or parcels in detail, and of course models cannot substitute for real observations.

c. Suggestions for future work

We believe the hydrate layer to be very important for possible future deposition of CO_2; however, the current experiment did not particularly illuminate the properties of the

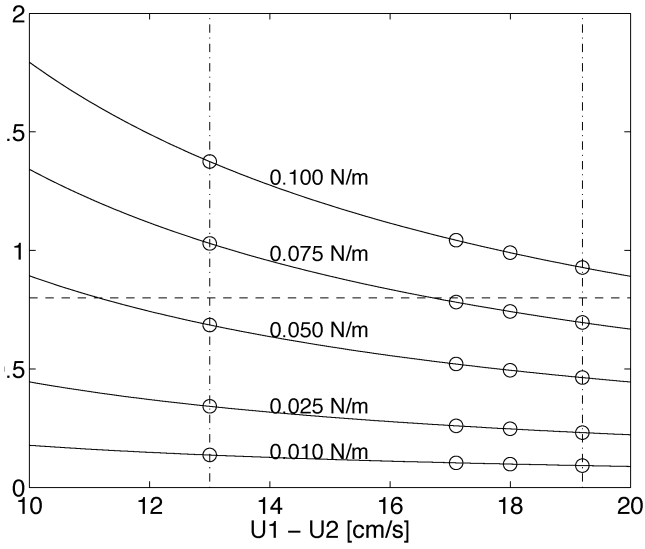

Figure 10. Wavelength with *maximum* growth rate (i.e. $\lambda^* = 2\pi/k^*$), as a function of shear, for different values of γ. The open circles indicate the calculated values of λ^* for the four different shear values in Figure 4. The horizontal dashed line corresponds to $\lambda^* \simeq 0.8$ cm, which is what we infer from Figure 4 and Figure 6.

hydrate. The hydrate layer is a *surface active layer,* and the repeated stretching and compression of this layer will lead to dissipation (Lucassen-Reynders and Lucassen, 1970), and wave decay. With a *longer* trough it would be possible to measure this decay.

The dispersion relation for the current experimental situation, Eq. 4, is *independent* of γ. A wave maker with smaller *amplitude* would allow for the excitations of high frequency waves with

$$\omega \gg \omega_c = \sqrt{\frac{2g\Delta\rho}{\rho}}\sqrt{\frac{g\Delta\rho}{\gamma}} \approx 7.4 \text{ rad/s}. \tag{8}$$

Then the wave maker could be used to *measure* γ. The density difference, $\Delta\rho$, determines the relative importance of the gravity term versus the capillary term in Eq. 4. Since ρ_{CO_2} is a known function of pressure, we can control this weighting by carefully selecting the depth for the experiment. For instance, an experimental depth of near the level where liquid CO_2 has the same density as seawater (i.e., around 3000 m) will give pure capillary waves.

5. Conclusion

We have found that waves propagating along the CO_2-seawater interface can be reasonably well described by the dispersion relation for deep water gravity waves. When sheared with a uniform current, waves are created on the interface. At 3940 m depth, when

the shear velocity exceeds a critical velocity of $v_c \simeq 17.6$ cm/s, the interface becomes unstable with breaking waves and CO_2 droplets torn from the wave crests. The mixing of CO_2 into the seawater will be greatly enhanced when the interface is turbulent. Doing a length-scale analysis we find that most energy is absorbed in modes with $\lambda \approx 0.8$ cm. This agrees reasonably well with the most unstable mode from Kelvin-Helmholtz instability if we assume the effective surface tension is $\gamma = 0.075$ N/m.

Acknowledgment. The experiment was carefully designed by the research group of Peter Brewer at MBARI, and Peter Brewer, Edward Peltzer and Peter Waltz are greatly acknowledged for this effort. The actual experiment hinged crucially on the skills of the ROV pilots, and their effort during the preparations and actual cruise is greatly acknowledged. The trough with wave maker and thruster was designed and built by ROV pilot Dale Graves.
Financial support was provided by an international research grant from the New Energy and Industrial Technology Organization (NEDO), Japan.

REFERENCES

Addison, P. S. 2002. The Wavelet Transform Handbook, Institute of Physics Publishing, 400 pp.

Alendal, G. and H. Drange. 2001. Two-phase, near field modeling of purposefully released CO_2 in the ocean. J. Geophys. Res., *106,* 1085–1091.

Anschutz, P., G. Blanc, F. Chatin, M. Geiller and M.-C. Pierret. 1999. Hydrographic changes during 20 years in the brine-filled basins of the Red Sea. Deep-Sea Res. I, *46,* 1779–1792.

Baines, P. G. 1995. Topographic Effects in Stratified Flows, *in* Monographs on Mechanics, Cambridge University Press, 482 pp.

Baklid, A., R. Korbøl and G. Owren. 1996. Sleipner vest CO_2 disposal: CO_2 injection into a shallow underground aquifer, *in* SPE Annual Technical Conference. SPE paper 36600, 1–9.

Brewer, P., G. Friederich, E. T. Peltzer and Franklin M. Orr, Jr. 1999. Direct experiment on the ocean disposal of fossil fuel CO_2. Science, *284,* 943–945.

Brewer, P., E. Peltzer, G. Friederich and G. Rehder. 2002. Experimental determination of the fate of rising CO_2 droplets in seawater. Environ. Sci. Technol., *36,* 5441–5446.

Brewer, P. G., E. T. Peltzer, P. Walz, I. Aya, K. Yamane, R. Kojima, Y. Nakajima, N. Nakayama, P. Haugan and T. Johannessen. 2005. Deep ocean experiments with fossil fuel carbon dioxide: Creation and sensing of a controlled plume at 4 km depth. J. Mar. Res., *63,* 9–33.

Cappelen, P., E. Viollier and A. Roychoudhury. 1998. Biogeochemical cycles of manganese and iron at the oxic-anoxic transition of a stratified marine basin (Orca Basin, Gulf of Mexico). Environ. Sci. Technol., *32,* 2931–2939.

Chandrasekhar, S. 1961. Hydrodynamic and Hydromagnetic Stability, Oxford University Press, 652 pp.

Drazin, P. G. and W. H. Reid. 1981. Hydrodynamic Stability, Cambridge University Press, 527 pp.

Fer, I. and P. M. Haugan. 2003. Dissolution from a liquid-CO_2 lake disposed in the deep ocean. Limnol. Oceanogr., *48,* 872–883.

Haugan, P. M. and G. Alendal. 2005. Turbulent diffusion and transport from a CO_2 lake in the deep ocean. J. Geoph. Res., (in press).

Haugan, P. M. and H. Drange. 1992. Sequestration of CO_2 in the deep ocean by shallow injection. Nature, *357,* 318–320.

Kantha, L. H. and C. A. Clayson. 2000. Small Scale Processes in Geophysical Fluid Flows, Academic Press, 888 pp.

Lee, S., L. Liang, D. Riestenberg, O. R. West, C. Tsouris and E. Adams. 2003. CO_2 hydrate composition for ocean carbon sequestration. Environ. Sci. Technol., *37,* 3701–3708.

Lucassen-Reynders, E. H. and J. Lucassen. 1970. Properties of capillary waves. Adv. in Colloid Interface Sci., *2,* 347–395.

Marchetti, C. 1977. On geoengineering and the CO_2 problem. Clim. Change, *1,* 59–68.

Martin, S. and P. Kauffman. 1981. A field and laboratory study of wave damping by grease ice. J. Glaciol., *27,* 283–313.

Mori, Y. H. 1998. Clathrate hydrate formation at the interface between liquid CO_2 and water phases—a review of rival models characterizing "hydrate films." Energy Convers. Mgmt., *39,* 1537–1557.

Rehder, G., S. Kirby, W. Durham, L. Stern, E. Peltzer, J. Pinkston and P. Brewer. 2004. Dissolution rates of pure methane hydrate and carbon-dioxide hydrate in undersaturated seawater at 1000 m depth. Geochim. Cosmochim. Acta, *68,* 285–292.

Sloan, E. D. 1998. Clathrate Hydrates of Natural Gases, Marcel Dekker, 705 pp.

Span, R. and W. Wagner. 1996. A new equation of state for carbon dioxide covering the fluid region from the triple-point temperature to 1100 K at pressures up to 800 MPa. J. Phys. Chem. Ref. Data, *25,* 1509–1596.

Uchida, T., R. Ohmura, S. Takeya, J. Nagao, H. Minagawa, T. Ebinuma and H. Narita. 2003. Estimations of interfacial tensions between liquid CO_2 and water from the sessile-drop observations, *in* Greenhouse Gas Control Technologies, Proc. 6th Int. Conf. Greenhouse Gas Control Technologies, II, J. Gale and Y. Kaya, eds., Elsevier, 1679–1682.

Yamane, K., I. Aya, S. Namie and H. Nariai. 2000. Strength of CO_2 hydrate membrane in sea water at 40 MPa. Ann. N.Y. Acad. Sci., *912,* 254–260.

Received: *4 August, 2004;* revised: *26 January, 2005.*